THE ASTROPHYSICAL JOURNAL, 440:116–127, 1995 February 10

RAPID POLARIZATION VARIABILITY IN INTENSE SOURCES

R. T. GANGADHARA AND V. KRISHAN
Indian Institute of Astrophysics, Bangalore-560 034, India
Received 1993 November 1; accepted 1994 August 12

ABSTRACT

We have recently reported the polarization changes of the intense electromagnetic radiation, in active galactic nuclei and pulsars, due to stimulated Raman scattering. In this paper, we show that the incident and the Raman-scattered radiation, when superimposed, exhibit highly complex and variable polarization patterns, some of which could account for the observed polarization variability in intense sources. Further, if the ratio of the frequencies of the incident and the scattered radiation is an irrational number, the electric field of the superimposed radiation traces a quasi-periodic rotation. The modulation of the Raman-scattered sideband modes, with even small perturbations due to the thermal radiation or the Raman cascade, would lead to chaotic rotation of the electric field of the superimposed radiation.

Subject headings: galaxies: active — instabilities — polarization — pulsars: general — radiation mechanisms: nonthermal

1. INTRODUCTION

Source models are constructed by assuming a synchrotron origin for the radiation in compact extragalactic radio sources to explain both the spectral and temporal behavior of intensity (e.g., van der Laan 1966; Blandford & Königl 1979), but polarization does not lend itself to such a straightforward explanation. The problems arise mainly from the observed ratio of circular to linear polarization; also, depolarization by a factor of 10 or more is often observed. It is important to determine whether this depolarization is a geometric effect or results from radiation-plasma interactions. There have only been very preliminary attempts to explain depolarization and microvariability using plasma mechanisms (Gangadhara & Krishan 1993; Krishan & Wiita 1994).

It is well known that Faraday effect and electron scattering can cause changes in polarization of an electromagnetic (EM) wave. In a plasma, the spectral components of radiation of finite bandwidth travel different path lengths, which may lead to depolarization. Any change in the direction of the magnetic field also manifests itself through polarization variation. The strong linear polarization observed in the radio as well as in the optical regions of the spectrum in a BL Lacertae object is believed to originate in the source itself. The fact that optically violently variables and NGC 1275 show similar polarization characteristics, suggests that BL Lac objects, quasars, and Seyfert galaxies have similar sources of energy. If so, then the lack of polarization in quasars and Seyfert galaxies could be due to depolarization effects (Stockman 1978). The rotation of the electric vector has been observed in the core-jet structure of 3C 454.3 (Cotton et al. 1984) and is interpreted to be due to the propagation of radiation in a medium of varying optical thickness.

Several pulsars exhibit one or more reversals of the sense of polarization through the pulse profile. The appearance of strong circular polarization (sometimes more than 50%) implies conversion of the elliptically polarized radiation somewhere along the propagation path. Apart from the appearance of circular polarization, however, pulsar magnetospheres do not appear to be magnetoactive (no generalized Faraday rotation is evident) (Cordes 1983). For pulsars in which the integrated profile is highly polarized, essentially all subpulses must likewise be highly polarized and have stable polarization characteristics. However, many pulsars have rather weakly polarized integrated profiles. Three possible reasons for low polarization (Manchester & Taylor 1977), apart from the Faraday rotation, electron scattering, and magnetic field orientations, are that the subpulses at a given longitude may (1) be themselves weakly polarized, (2) be divisible into groups with orthogonal polarization, or (3) have randomly varying position angles and sense of circular polarization.

Analysis of the AGN data by the University of Michigan (Aller, Aller, & Hughes 1991) in the centimeter-wavelength regime showed both flux and linear polarization variability, and in addition, polarization frequently exhibited position angle swings and large changes in percentage of polarization. To explain these observational results one incorporates shock models with special geometries, whereas stimulated Raman scattering (SRS), without invoking many constraints, can explain these results (Gangadhara & Krishan 1993; Krishan & Gangadhara 1992). The physics of SRS in a plasma has been explained in many papers and books (e.g., Drake et al. 1974; Liu & Kaw 1976; Hasegawa 1978; Kruer 1988; Krishan & Wiita 1990; Gangadhara & Krishan 1992, 1993).

Sillanpää, Nilsson, & Takalo (1991) observed rotation of polarization position angle linearly 55° in 5 hr, in all five colors, in the optical regime of OJ 287. This is the fastest ever observed position angle swing at optical regions in OJ 287 or in blazars. It is difficult to explain this observed position angle swing with shocks in a jet model.

A powerful collective emission occurs when relativistic electron beams with density greater than 1% of the background plasma density scatter off coherently from concentrations of electrostatic plasma waves (cavitons) (Benford 1992). The polarization of the emitted radiation depends on the orientation and shape of cavitons. Assuming the usual power-law spectrum for electron energies, polarization features mimic synchrotron radiation (Baker et al. 1988; Weatherall & Benford 1991). Several coherent processes, such as (1) emission from bunches of relativistic electron beams (Ruderman & Sutherland 1975), (2) curvature radiation (Gil & Snakowski 1990a, b; Asséo, Pellat, & Sol 1980), and (3) parallel acceleration mechanisms (Melrose 1978), have been proposed for the radio emission from pulsars. On the other hand, the role of the coherent emission processes in the generation of continuum emission of the

quasar was emphasized long ago (Burbidge & Burbidge 1967) and has now begun to receive the attention it deserves (Lesch & Pohl 1992; Krishan & Wiita 1990; Baker et al. 1988).

There have been some attempts to explain absorption and spectral modification of the radiation through its interaction with the plasma in accretion disks and emission-line regions using collective plasma processes (Beal 1990; Krishan & Wiita 1990; Benford 1992; Gangadhara & Krishan 1992; Gangadhara, Krishan, & Shukla 1993). In an earlier paper (Gangadhara & Krishan 1993), we demonstrated how SRS can bring about fast and varied changes in the polarization pattern. In this paper, we demonstrate the complexity and the variability of the polarization pattern that can result from the superposition of the incident radiation with its SRS component. It is essential to study the polarization properties of the superimposed radiation since, more often than not, that is what may be observed. The characteristic time of polarization variation is governed by the scattering time or the growth time of the Raman instability. Polarization changes through SRS may take place in accretion disks, the emission-line regions, and the intercloud medium of active galactic nuclei (AGNs), and also in the emission region of pulsars. In § 2, we give the dispersion relation describing the SRS of an EM wave. In § 3, we numerically solve the dispersion relation to find the value of the growth rate of the SRS instability. We briefly discuss the route to chaotic polarization changes from quasi-periodic ones in § 4, and end the paper with conclusions.

2. POLARIZATION CHARACTERISTICS OF THE SUPERIMPOSED RADIATION

Consider a large-amplitude elliptically polarized EM wave $(\boldsymbol{k}_i, \omega_i)$, with an electric field

$$\boldsymbol{E}_i = \epsilon_i[\cos(\boldsymbol{k}_i \cdot \boldsymbol{r} - \omega_i t)\hat{\boldsymbol{e}}_x + \alpha_i \cos(\boldsymbol{k}_i \cdot \boldsymbol{r} - \omega_i t + \delta_i)\hat{\boldsymbol{e}}_y] , \tag{1}$$

propagating in a plasma with equilibrium density n_0 and temperature T_e.

Let $n_e = n_0 + \delta n_e$ be the electron plasma density with $\delta n_e = \delta n \cos(\boldsymbol{k} \cdot \boldsymbol{r} - \omega t + \delta_e)$. The coupling between the EM wave and the plasma density perturbation $\delta n_e(\boldsymbol{k}, \omega)$ is nonlinear because of the ponderomotive force ($\propto \nabla E_i^2$). Consequently, density perturbations grow up and lead to currents at $(\boldsymbol{k}_i \pm \boldsymbol{k}, \omega_i \pm \omega)$. These currents will generate mixed electromagnetic-electrostatic sideband modes at $(\boldsymbol{k}_i \pm \boldsymbol{k}, \omega_i \pm \omega)$. The sideband modes, in turn, interact with the incident wave field, producing a ponderomotive force which amplifies the original density perturbation. Thus, there is a positive feedback system which leads to an instability.

The electric field $\boldsymbol{E}_s$ of the EM wave scattered through an angle ϕ_s with respect to $\boldsymbol{k}_i$ can be written as

$$\boldsymbol{E}_s = \epsilon_s[\cos(\boldsymbol{k}_s \cdot \boldsymbol{r} - \omega_s t)\hat{\boldsymbol{e}}'_x + \alpha_s \cos(\boldsymbol{k}_s \cdot \boldsymbol{r} - \omega_s t + \delta_s)\hat{\boldsymbol{e}}'_y] . \tag{2}$$

Figure 1 shows the directions of $\boldsymbol{k}_i$ and $\boldsymbol{k}_s$ in the orthogonal coordinate systems $(\hat{\boldsymbol{e}}_x, \hat{\boldsymbol{e}}_y, \hat{\boldsymbol{e}}_z)$ and $(\hat{\boldsymbol{e}}'_x, \hat{\boldsymbol{e}}'_y, \hat{\boldsymbol{e}}'_z)$. The coordinate system $(\hat{\boldsymbol{e}}'_x, \hat{\boldsymbol{e}}'_y, \hat{\boldsymbol{e}}'_z)$ is rotated through an angle ϕ_s about an axis parallel to $\hat{\boldsymbol{e}}_y$. Here, $\boldsymbol{k}_i \| \hat{\boldsymbol{e}}_z$, $\boldsymbol{k}_s \| \hat{\boldsymbol{e}}'_z$ and $\hat{\boldsymbol{e}}'_y \| \hat{\boldsymbol{e}}_y$. The unit vectors are related by

$$\hat{\boldsymbol{e}}'_x = \cos(\phi_s)\hat{\boldsymbol{e}}_x - \sin(\phi_s)\hat{\boldsymbol{e}}_z , \qquad \hat{\boldsymbol{e}}'_y = \hat{\boldsymbol{e}}_y , \qquad \hat{\boldsymbol{e}}'_z = \sin(\phi_s)\hat{\boldsymbol{e}}_x + \cos(\phi_s)\hat{\boldsymbol{e}}_z . \tag{3}$$

The scattered wave in the coordinate system $(\hat{\boldsymbol{e}}_x, \hat{\boldsymbol{e}}_y, \hat{\boldsymbol{e}}_z)$ is given by

$$\boldsymbol{E}_s = \epsilon_s\{\cos(\boldsymbol{k}_s \cdot \boldsymbol{r} - \omega_s t)[\cos(\phi_s)\hat{\boldsymbol{e}}_x - \sin(\phi_s)\hat{\boldsymbol{e}}_z] + \alpha_s \cos(\boldsymbol{k}_s \cdot \boldsymbol{r} - \omega_s t + \delta_s)\hat{\boldsymbol{e}}_y\} . \tag{4}$$

The wave equation for the scattered EM wave is given by

$$\left(\nabla^2 - \frac{1}{c^2}\frac{\partial^2}{\partial t^2}\right)\boldsymbol{E}_s = \frac{4\pi}{c^2}\frac{\partial \boldsymbol{J}}{\partial t} , \tag{5}$$

where c is the velocity of light and $\boldsymbol{J}$ is the current density. The components of the current density are $J_1 = -e(n_0 + \delta n_e)u_{e1}$, $J_2 = -e(n_0 + \delta n_e)u_{e2}$, and $J_3 = -e(n_0 + \delta n_e)u_{e3}$, where u_{e1}, u_{e2}, and u_{e3} are the components of the oscillation velocity $\boldsymbol{u}_e$ of electrons in the radiation fields $\boldsymbol{E}_i$ and $\boldsymbol{E}_s$.

In component form, equation (5) can be written as

$$D_s E_1 = -\frac{2\pi e^2}{m_0}\epsilon_i \delta n\left[\frac{\omega_-}{\omega_i}\cos(\boldsymbol{k}_- \cdot \boldsymbol{r} - \omega_- t - \delta_e) + \frac{\omega_+}{\omega_i}\cos(\boldsymbol{k}_+ \cdot \boldsymbol{r} - \omega_+ t + \delta_e)\right] , \tag{6}$$

$$D_s E_2 = -\frac{2\pi e^2}{m_0}\alpha_i \epsilon_i \delta n\left[\frac{\omega_-}{\omega_i}\cos(\boldsymbol{k}_- \cdot \boldsymbol{r} - \omega_- t + \delta_i - \delta_e) + \frac{\omega_+}{\omega_i}\cos(\boldsymbol{k}_+ \cdot \boldsymbol{r} - \omega_+ t + \delta_i + \delta_e)\right] , \tag{7}$$

and

$$D_s E_3 = 0 , \tag{8}$$

where $E_1 = \epsilon_s \cos(\phi_s)\cos(\boldsymbol{k}_s \cdot \boldsymbol{r} - \omega_s t)$, $E_2 = \alpha_s \epsilon_s \cos(\boldsymbol{k}_s \cdot \boldsymbol{r} - \omega_s t + \delta_s)$, $E_3 = -\epsilon_s \sin(\phi_s)\cos(\boldsymbol{k}_s \cdot \boldsymbol{r} - \omega_s t)$, and $D_s = k_s^2 c^2 - \omega_s^2 + \omega_{pe}^2$. Here $\omega_{pe} = (4\pi n_0 e^2/m_0)^{1/2}$ is the plasms frequency. In equation (8), $D_s \approx 0$.

The scattered radiation will have both the Stokes ($s = -$) and anti-Stokes ($s = +$) modes. The expressions $D_\pm = k_\pm^2 c^2 - \omega_\pm^2 + \omega_{pe}^2 \approx 0$ are the dispersion relations for the Stokes mode $(\boldsymbol{k}_-, \omega_-)$ and the anti-Stokes mode $(\boldsymbol{k}_+, \omega_+)$, when the following resonant conditions are satisfied:

$$\omega_i - \omega = \omega_- , \qquad \boldsymbol{k}_i - \boldsymbol{k} = \boldsymbol{k}_- ,$$
$$\omega_i + \omega = \omega_+ , \qquad \boldsymbol{k}_i + \boldsymbol{k} = \boldsymbol{k}_+ . \tag{9}$$

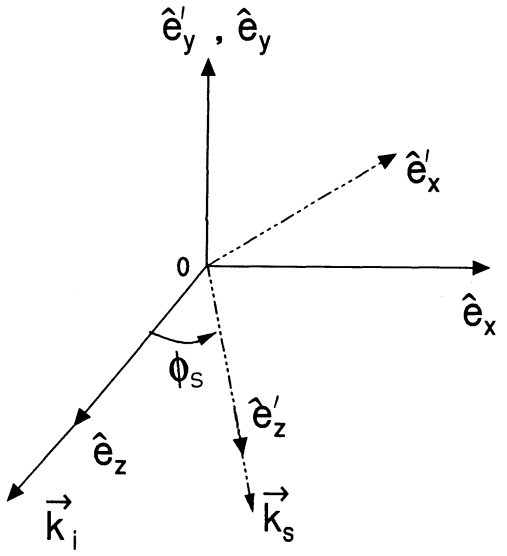

FIG. 1

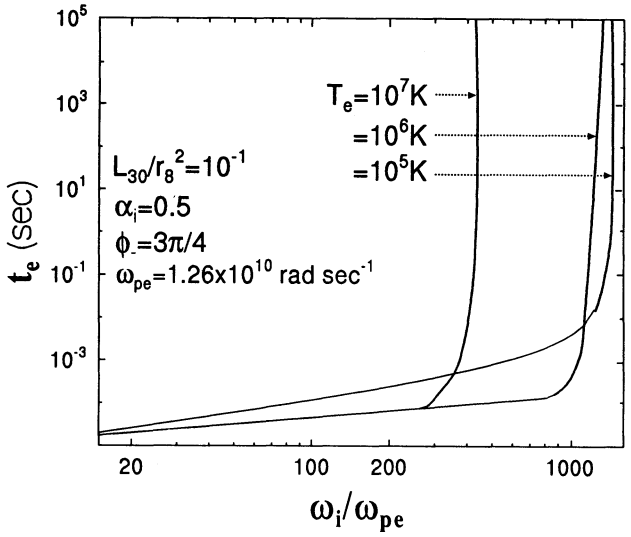

FIG. 2

FIG. 1.—Wave vectors and the electric fields of the incident and the scattered radiation
FIG. 2.—e-folding time $t_e = 1/\Gamma$ vs. the frequency of the incident wave (ω_i/ω_{pe}) at the electron plasma temperature $T_e = 10^5, 10^6$, and 10^7 K

Multiplying equation (6) on both sides by $\cos(\boldsymbol{k}_i \cdot \boldsymbol{r} - \omega_i t)$ and neglecting the terms containing $(2\boldsymbol{k}_i, 2\omega_i)$ as being nonresonant, we get

$$D_\pm \epsilon_\pm \cos(\phi_\pm) \cos(\boldsymbol{k} \cdot \boldsymbol{r} - \omega t) = -\frac{4\pi e^2}{m_0} \epsilon_i \delta n \cos(\boldsymbol{k} \cdot \boldsymbol{r} - \omega t + \delta_e) . \tag{10}$$

Similarly, if we multiply equation (7) by $\cos(\boldsymbol{k}_i \cdot \boldsymbol{r} - \omega_i t + \delta_i)$, we obtain

$$D_\pm \alpha_\pm \epsilon_\pm \cos[\boldsymbol{k} \cdot \boldsymbol{r} - \omega t \pm (\delta_\pm - \delta_i)] = -\frac{4\pi e^2}{m_0} \alpha_i \epsilon_i \delta n \cos(\boldsymbol{k} \cdot \boldsymbol{r} - \omega t + \delta_e) . \tag{11}$$

Similar to equations (9), this gives the following conditions between the phases:

$$\delta_\pm = \delta_i \pm \delta_e . \tag{12}$$

Dividing equation (11) by equation (10), we have

$$\begin{aligned} \alpha_\pm &= \alpha_i \cos(\phi_\pm) , \qquad \text{for } \delta_e = 0 ; \\ &= -\alpha_i \cos(\phi_\pm) , \qquad \text{for } \delta_e = \pi . \end{aligned} \tag{13}$$

Now, the electric fields $\boldsymbol{E}_\pm$ of the EM waves scattered through an angle $\phi_\pm$ with respect to $\boldsymbol{k}_i$ can be written as (for both $\delta_e = 0$ and π)

$$\boldsymbol{E}_\pm = \epsilon_\pm [\cos(\boldsymbol{k}_\pm \cdot \boldsymbol{r} - \omega_\pm t)\hat{\boldsymbol{e}}'_x + \alpha_i \cos(\phi_\pm) \cos(\boldsymbol{k}_\pm \cdot \boldsymbol{r} - \omega_\pm t + \delta_i)\hat{\boldsymbol{e}}'_y] .$$

For $\phi_\pm \leq \pi/2$, the sense of rotation of the scattered waves will be same as for the incident wave. But, when $\phi_\pm > \pi/2$, the scattered waves will reverse their sense of rotation compared to the incident wave, as we will discuss in later sections.

If we multiply equation (10) by ϵ_i and equation (11) by $\alpha_i \epsilon_i$, after subtracting we find

$$(\alpha_i \alpha_\pm - \cos\phi_\pm)\epsilon_i \epsilon_\pm = -\frac{4\pi e^2}{m_0} \epsilon_i^2 (1 + \alpha_i^2) \delta n \frac{1}{D_\pm} , \tag{14}$$

where $\delta_e = \pi$ has been used.

Now, we have to determine the electron density perturbation δn. We neglect the ions' response because of their larger mass compared to that of the electrons. With the inclusion of the ponderomotive force as a driving force, the Vlasov equation for the low-frequency response of electrons can then be written as

$$\frac{\partial f}{\partial t} + \boldsymbol{v} \cdot \nabla f + \frac{1}{m_0} (e\nabla\phi - \nabla\psi) \cdot \frac{\partial f}{\partial \boldsymbol{v}} = 0 , \tag{15}$$

where $\phi(\boldsymbol{r}, t)$ is the scalar potential associated with the electrostatic waves, $f(\boldsymbol{r}, \boldsymbol{v}, t)$ is the particle distribution function, and $\psi(\boldsymbol{r}, t)$ is the ponderomotive potential.

Linearizing equation (15) with $f(\boldsymbol{r}, \boldsymbol{v}, t) = f_0(\boldsymbol{v}) + \delta f_e(\boldsymbol{r}, \boldsymbol{v}, t)$, we get

$$\frac{\partial(\delta f_e)}{\partial t} + \boldsymbol{v} \cdot \nabla(\delta f_e) + \frac{1}{m_0}(e\nabla\phi - \nabla\psi) \cdot \frac{\partial f_0}{\partial \boldsymbol{v}} = 0 , \tag{16}$$

where $\delta f_e = \delta f \cos(\boldsymbol{k} \cdot \boldsymbol{r} - \omega t + \delta_e)$. The ponderomotive force of the radiation field is given by $\boldsymbol{F}_\omega = -\nabla\psi$. It depends quadratically on the amplitude and leads to a slowly varying longitudinal field, corresponding physically to radiation pressure, which leads to slow longitudinal motions and modifies the density. The ponderomotive potential is given by

$$\begin{aligned}\psi &= \frac{e^2}{2m_0}\left\langle\left(\mathrm{Re}\left|\frac{\boldsymbol{E}_i}{i\omega_i} + \frac{\boldsymbol{E}_-}{i\omega_-} + \frac{\boldsymbol{E}_+}{i\omega_+}\right|\right)^2\right\rangle_\omega \\ &= \frac{e^2}{2m_0\omega_i^2}[\epsilon_i\epsilon_- \cos(\phi_-)\cos(\boldsymbol{k} \cdot \boldsymbol{r} - \omega t) + \alpha_i\alpha_-\epsilon_i\epsilon_- \cos(\boldsymbol{k} \cdot \boldsymbol{r} - \omega t + \delta_i - \delta_-) \\ &\quad + \epsilon_i\epsilon_+ \cos(\phi_+)\cos(\boldsymbol{k} \cdot \boldsymbol{r} - \omega t) + \alpha_i\alpha_+\epsilon_i\epsilon_+ \cos(\boldsymbol{k} \cdot \boldsymbol{r} - \omega t + \delta_+ - \delta_i)] .\end{aligned} \tag{17}$$

The angle bracket $\langle\ \rangle_\omega$ represents the ω frequency component of an average over the fast timescale ($\omega_i \gg \omega$).

To determine ϕ self-consistently we use the Poisson equation, which gives

$$\phi = -\frac{4\pi e}{k^2}(\delta n_e) . \tag{18}$$

Now, substituting the expressions for δf_e, δn_e, ϕ, and ψ into equation (16), we get

$$\delta f + \frac{4\pi e^2}{m_0 k^2}\left\{\delta n + \frac{k^2}{8\pi m_0\omega_i^2}\left[\epsilon_i\epsilon_- \cos(\phi_-)\mu + \epsilon_i\epsilon_+ \cos(\phi_+)\mu + \alpha_i\alpha_-\epsilon_i\epsilon_- \frac{\sin(\boldsymbol{k} \cdot \boldsymbol{r} - \omega t + \delta_i - \delta_-)}{\sin(\boldsymbol{k} \cdot \boldsymbol{r} - \omega t + \delta_e)} + \alpha_i\alpha_+\epsilon_i\epsilon_+ \frac{\sin(\boldsymbol{k} \cdot \boldsymbol{r} - \omega t + \delta_+ - \delta_i)}{\sin(\boldsymbol{k} \cdot \boldsymbol{r} - \omega t + \delta_e)}\right]\right\}\frac{\boldsymbol{k} \cdot (\partial f_0/\partial \boldsymbol{v})}{\omega - \boldsymbol{k} \cdot \boldsymbol{v}} = 0 , \tag{19}$$

where $\mu = \sin(\boldsymbol{k} \cdot \boldsymbol{r} - \omega t)/\sin(\boldsymbol{k} \cdot \boldsymbol{r} - \omega t + \delta_e)$.

Equation (19) shows that $\delta_\pm = \delta_i \pm \delta_e$ and $\delta_e = 0$ or π. We obtain, for $\delta_e = \pi$,

$$\delta f = -\frac{4\pi e^2}{m_0 k^2}\left(\delta n + \frac{k^2}{8\pi m_0\omega_i^2} A\right)\frac{\boldsymbol{k} \cdot (\partial f_0/\partial \boldsymbol{v})}{\omega - \boldsymbol{k} \cdot \boldsymbol{v}} , \tag{20}$$

where $A = (\alpha_i\alpha_- - \cos\phi_-)\epsilon_i\epsilon_- + (\alpha_i\alpha_+ - \cos\phi_+)\epsilon_i\epsilon_+$. The density perturbation δn is given by

$$\delta n = \int_{-\infty}^{\infty} n_0\,\delta f\,d\boldsymbol{v} = -\left(\delta n + \frac{k^2}{8\pi m_0\omega_i^2} A\right)\chi_e , \tag{21}$$

where

$$\chi_e = \frac{\omega_{pe}^2}{k^2}\int_{-\infty}^{\infty} \frac{\boldsymbol{k} \cdot (\partial f_0/\partial \boldsymbol{v})}{\omega - \boldsymbol{k} \cdot \boldsymbol{v}}\,d\boldsymbol{v} \tag{22}$$

is the electron susceptibility function (Liu & Kaw 1976; Fried & Conte 1961). From equation (21) we have

$$\left(1 + \frac{1}{\chi_e}\right)\delta n = -\frac{k^2}{8\pi m_0\omega_i^2} A . \tag{23}$$

Substituting equation (23) for δn into equation (14), we obtain

$$1 + \frac{1}{\chi_e} = \frac{v_0^2 k^2}{2}\left(\frac{1}{D_-} + \frac{1}{D_+}\right) , \tag{24}$$

where $v_0 = e\epsilon_i\sqrt{1 + \alpha_i^2}/m_0\omega_i$ is the quiver velocity of electrons in the field of the incident EM wave. Equation (24) is the dispersion relation for SRS of the EM wave (see eq. [1]) in a plasma medium, and an exactly similar expression can be obtained using $\delta_e = 0$.

The SRS instability resonantly excites only when the frequency and wave-number matching conditions (see eq. [9]) are satisfied. The simplest stimulated scattering process is the one involving only one high-frequency sideband, i.e., the Stokes component ($\boldsymbol{k}_-$, ω_-). Thus, we consider a case where $D_- \approx 0$ and $D_+ \neq 0$. i.e., the anti-Stokes component ($\boldsymbol{k}_+$, ω_+) is nonresonant. This approximation is justified as long as $\omega \ll (c^2\boldsymbol{k}_i \cdot \boldsymbol{k}/\omega_i)$; it breaks down for very small $\boldsymbol{k}$ (i.e., for long-wavelength electrostatic perturbations) or if $\boldsymbol{k}$ is nearly perpendicular to $\boldsymbol{k}_i$.

The value of k is approximately $2k_i$, corresponding to backward scattering ($\phi_- = \pi$), and for forward scattering ($\phi_- = 0$) it is approximately ω_{pe}/c. Thus, the growth rate of the instability attains its maximum value for backscatter. For the case of backscattering, $D_-(\boldsymbol{k}_-, \omega_-) \approx 2\omega_i(\omega - c^2\boldsymbol{k}_i \cdot \boldsymbol{k}/\omega_i + c^2k^2/2\omega_i) \approx 0$ for $\omega_i \gg \omega$. The dispersion relation for primarily backscatter is, therefore,

$$1 + \frac{1}{\chi_e} = \frac{1}{4}\frac{v_0^2 k^2}{\omega_i(\omega - \Delta)}, \tag{25}$$

where

$$\Delta = \boldsymbol{k} \cdot \boldsymbol{v}_g - \frac{k^2c^2}{2\omega_i}, \tag{26}$$

with $\boldsymbol{v}_g = \boldsymbol{k}_i c^2/\omega_i$. From the equation (25), we can derive the threshold and the growth rate for the SRS instability. For $\omega^2 \approx \omega_e^2 = \omega_{pe}^2 + (3/2)k^2v_T^2$, the natural frequency of the plasma wave, and $\omega_-^2 \approx \omega_{pe}^2 + c^2(\boldsymbol{k}_i - \boldsymbol{k})^2$, equation (25) can be written as

$$(\omega - \omega_e + i\Gamma_e)(\omega - \omega_e + i\Gamma_-) = -\frac{v_0^2 k^2 \omega_{pe}}{8\omega_i}, \tag{27}$$

where

$$\Gamma_e = \frac{\sqrt{\pi}}{2}\frac{\omega_{pe}}{(k\lambda_{De})^3}\exp\left[-\frac{1}{2(k\lambda_{De})^2} - \frac{3}{2}\right] + \nu_e \tag{28}$$

is the damping rate of the electron plasma wave, $\nu_e = 3.632 n_e \ln\Lambda/T_e^{3/2}$ is the electron collision frequency, and the Coulomb logarithm $\ln\Lambda \approx 10$. Here, $\Gamma_- = \omega_{pe}^2\nu_e/2\omega_-^2$ is the collisional damping rate of the scattered EM wave. Setting $\omega = \omega_e + i\Gamma$ and solving equation (27) for the growth rate Γ, we find

$$\Gamma = -\frac{1}{2}(\Gamma_e + \Gamma_-) \pm \frac{1}{2}\sqrt{(\Gamma_e - \Gamma_-)^2 + \frac{v_0^2 k^2 \omega_{pe}}{2\omega_i}}. \tag{29}$$

Setting $\Gamma = 0$, we obtain the threshold condition for the excitation of Raman scattering;

$$\left(\frac{v_0}{c}\right)_{thr} = \sqrt{\frac{2\Gamma_e\Gamma_-}{\omega_i\omega_{pe}}}. \tag{30}$$

3. NUMERICAL SOLUTION OF EQUATION (24)

When $k_l\lambda_{De} \approx 0.4$, the electron plasma wave is strongly damped; in this limit, it is not possible to expand $\chi_e(\omega, k)$ into an asymptotic series. The regime $k_t\lambda_{De} \approx 0.4$ corresponds to the transition region between SRS and stimulated Compton scattering (SCS) (Gangadhara & Krishan 1992). Therefore, using $\omega = \omega_e + i\Gamma$, we numerically solve equation (24) including all the damping effects.

The energy density of the incident field and the luminosity L of the source are related by

$$\frac{1}{8\pi}\epsilon_i^2(1 + \alpha_i^2) = \frac{L}{4\pi r^2 c}, \tag{31}$$

where r is the distance between source of radiation and plasma. Therefore, the quiver velocity of electrons is given by

$$v_0 = \frac{e}{m_0}\left(\frac{2L}{r^2c}\right)^{1/2}\frac{1}{\omega_i}. \tag{32}$$

4.1. *In Pulsars*

The typical values of the plasma and radiation parameters at a distance $r = 100R_{NS} = r_8 \times 10^8$ cm (neutron star radius $R_{NS} \approx 10$ km) in a pulsar are electron density $n_e = n_{10} \times 10^{10}$ cm^{-3}, temperature $T_e = T_5 \times 10^5$ K, and luminosity $L = L_{30} \times 10^{30}$ ergs s^{-1} in the band $\Delta\nu < \nu = 600$ MHz (Gangadhara et al. 1993).

We know from the observations of pulsar PSR 1133+16 by Cordes (1983) that flux $I_i = 10^{-20}$ ergs cm^{-2} s^{-1} Hz^{-1} at the radio frequency $\nu_i = 600$ MHz. To find the relation between the incident flux I_i and the scattered flux I_- we use the condition for conservation of wave energy within systems of waves, the Manley–Row relation (Weiland & Wilhelmsson 1977), given by

$$\frac{I_i}{\omega_i} = \frac{I_-}{\omega_-}. \tag{33}$$

For $\omega_i = 1.1\omega_-$, we get $I_- \approx 0.9I_i$.

The scattered radiation, detected by the detector, will have the contributions from the incident mode, Stokes mode, and weakly excited anti-Stokes mode. If we superimpose incident and Stokes modes, we get the electric field $\boldsymbol{E}_t$ of the superposed wave

$$\boldsymbol{E}_t = \boldsymbol{E}_0 + \boldsymbol{E}_- = \epsilon_i\left\{\cos(\boldsymbol{k}_i\cdot\boldsymbol{r}-\omega_i t)+\frac{\cos(\phi_-)}{\sqrt{2}}\cos(\boldsymbol{k}_-\cdot\boldsymbol{r}-\omega_- t)\right\}\hat{\boldsymbol{e}}_x$$
$$+\alpha_i\epsilon_i\left\{\cos(\boldsymbol{k}_i\cdot\boldsymbol{r}-\omega_i t+\delta_i)+\frac{\cos(\phi_-)}{\sqrt{2}}\cos(\boldsymbol{k}_-\cdot\boldsymbol{r}-\omega_- t+\delta_i)\right\}\hat{\boldsymbol{e}}_y-\epsilon_i\frac{\sin(\phi_-)}{\sqrt{2}}\cos(\boldsymbol{k}_-\cdot\boldsymbol{r}-\omega_- t)\hat{\boldsymbol{e}}_z\,. \quad (34)$$

Figure 2 shows the e-folding time $t_e = 1/\Gamma$ as a function of ω_i/ω_{pe} at the different values of electron temperature T_e ($=10^5$, 10^6, and 10^7 K) for forward SRS of the incident wave. The frequency of the scattered EM wave is $\omega_- = \omega_i - \omega_e$. One recalls that at high temperatures the electron plasma wave experiences a small collisional damping but large Landau damping. Here the fast rise in t_e is obtained due to large Landau damping. It is seen that a reversal in the sense of polarization changes can take place over a timescale lying between 10^{-4} and 10^{-5} s.

In Figure 3, we have plotted e-folding time as a function of the scattering angle ϕ_-. It shows SRS occurs very efficiently, when the incident wave undergoes backscattering. The growth rate of SRS instability is a strong function of $\cos\phi_-$, and scattering angles corresponding to larger growth rates will be naturally favored.

Figure 4 shows the elliptically polarized incident wave with electric field $\boldsymbol{E}_i$ in the x-y plane. If the sense of rotation of $\boldsymbol{E}_i$ is counterclockwise, due to SRS the scattered wave with electric field $\boldsymbol{E}_-$ in the x'-y' plane will be elliptically polarized with a clockwise sense of rotation.

Figure 5 shows the parametric plot of instantaneous variations of electric fields $\boldsymbol{E}_i$, $\boldsymbol{E}'_-$, and $\boldsymbol{E}_t$ with respect to time t, where $\epsilon_i = 73L_{30}/r_8^2$ statvolt cm^{-1}, $L_{30} = 1$, $r_8 = 1$, and $\omega_i = 3.768\times10^9$ rad s^{-1}. Figure 5*a* shows the linearly polarized incident-wave electric field $\boldsymbol{E}_i$ in the x-y plane. Figure 5*b* shows the linearly polarized scattered-wave electric field $\boldsymbol{E}'_-$ in the x'-y' plane. The electric field $\boldsymbol{E}_t$ of the superimposed wave with $\omega_i = 1.1\omega_-$ has all three nonzero components in the $(\hat{\boldsymbol{e}}_x, \hat{\boldsymbol{e}}_y, \hat{\boldsymbol{e}}_z)$ coordinate system. Figure 5*c* shows the parametric plot of E_{tx} versus E_{ty} in the x-y plane. Similarly, Figure 5*d* is the parametric plot of E_{tx} versus E_{tz} in the x-z plane, and Figure 5*e* is the parametric plot of E_{ty} versus E_{tz} in the y-z plane. The curves in Figures 5*d* and 5*e* show a new type of polarization, with period of rotation of $T = 11\times 2\pi/\omega_-$.

Figure 6 shows the parametric plot of the instantaneous variations of the electric fields $\boldsymbol{E}_i$, $\boldsymbol{E}'_-$, and $\boldsymbol{E}_t$ with respect to time t. Here the incident (Fig. 6*a*) and the scattered (Fig. 6*b*) waves are elliptical, while the superposed wave has a new complex polarization pattern as indicated by the curves in Figures 6*c*–6*e*. Here the electric field vector $\boldsymbol{E}_t$ shows multiple reversals in its sense of rotation in all three planes.

Figure 7 shows the parametric plot of instantaneous variations of electric fields $\boldsymbol{E}_i$, $\boldsymbol{E}'_-$, and $\boldsymbol{E}_t$ with respect to time t. Here the incident wave is circularly polarized (Fig. 7*a*) and the scattered wave is elliptically polarized (Fig. 7*b*), but the superimposed wave again has a complex pattern of polarization indicated by the different curves in Figures 7*c*–7*e*, with period $T = 11\times 2\pi/\omega_-$.

In Figures 5, 6, and 7, if we take the frequency ratio $\omega_i/\omega_- = 4.1/3$, an irrational number, then $\boldsymbol{E}_t$ shows quasi-periodic rotation with a period of each cycle of $T = 13.666\cdots\times 2\pi/\omega_-$. By varying the time variable t from 0 to $15T$, we find Figure 5*c* remains the same as Figure 8*a*, while Figure 5*d* changes to Figure 8*b* and Figure 5*e* changes to Figure 8*c*. Similarly, Figures 6*c*–6*e* change to

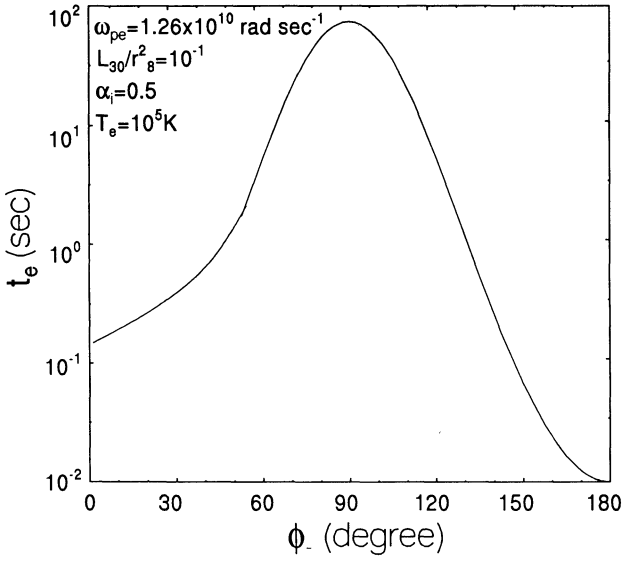

FIG. 3

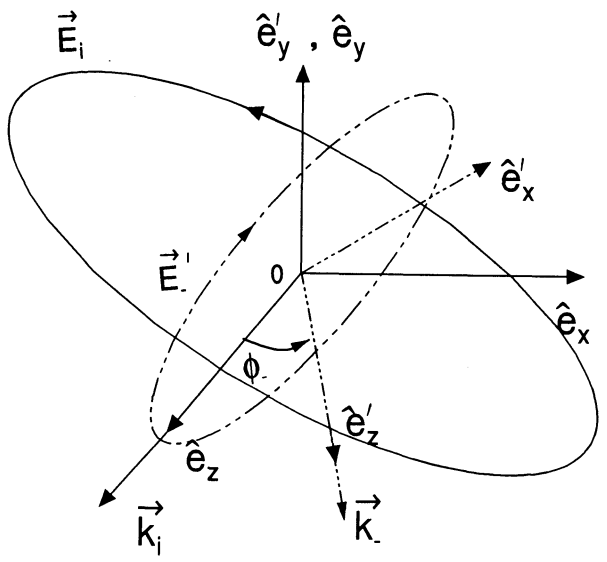

FIG. 4

FIG. 3.—e-folding time $t_e = 1/\Gamma$ vs. the scattering angle ϕ_-

FIG. 4.—Electric fields of incident and scattered EM waves in the coordinate systems $(\hat{\boldsymbol{e}}_x, \hat{\boldsymbol{e}}_y, \hat{\boldsymbol{e}}_z)$ and $(\hat{\boldsymbol{e}}_x, \hat{\boldsymbol{e}}_y, \hat{\boldsymbol{e}}_z)$, respectively. The incident-wave ellipse is in the x-y plane with $\boldsymbol{k}_i$ parallel to $\hat{\boldsymbol{e}}_z$, and the scattered-wave ellipse (*dash–double-dotted*) is in the x'-y' plane with $\boldsymbol{k}_-$ parallel to $\hat{\boldsymbol{e}}'_z$.

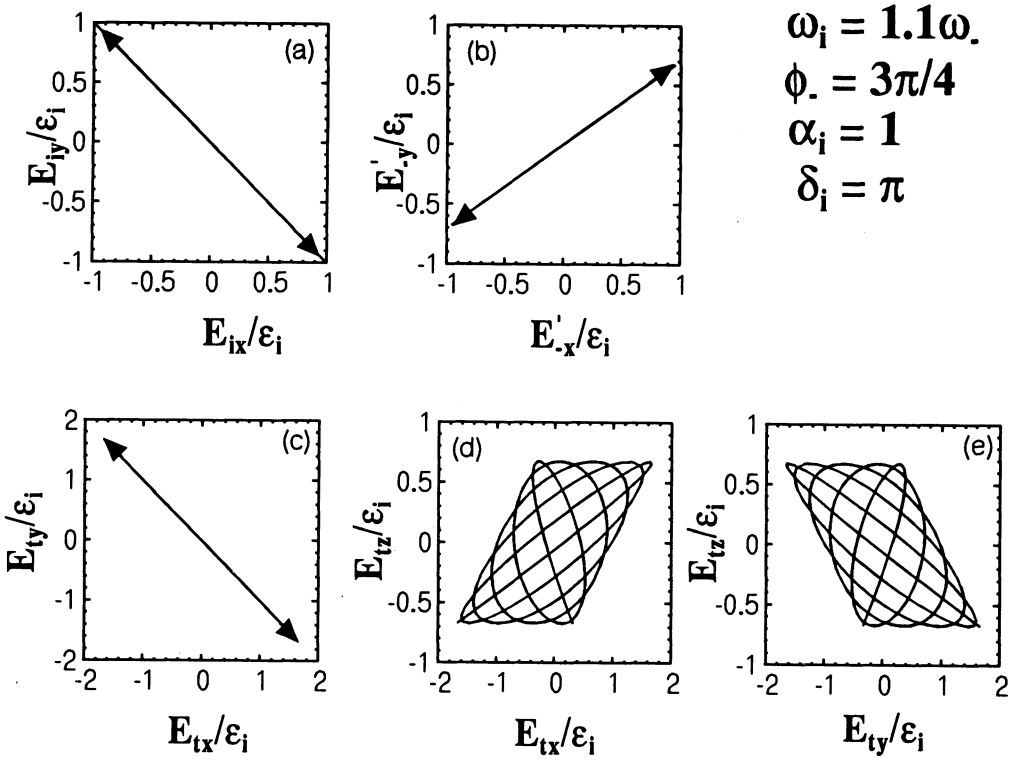

FIG. 5.—Parametric plot of electric fields E_i, E'_-, and E_t with respect to time t. Linearly polarized incident wave E_i in the x-y plane (a); linearly polarized scattered wave E'_- in the x'-y' plane (b); superimposed wave E_t in the x-y plane (c), x-z plane (d), and y-z plane (e). Here $\epsilon_i = 73L_{30}/r_8^2$ statvolt cm^{-1}, $L_{30} = 1$, $r_8 = 1$, $\omega_- = \omega_i/1.1$, and $\omega_i = 3.768 \times 10^9$ rad s^{-1}.

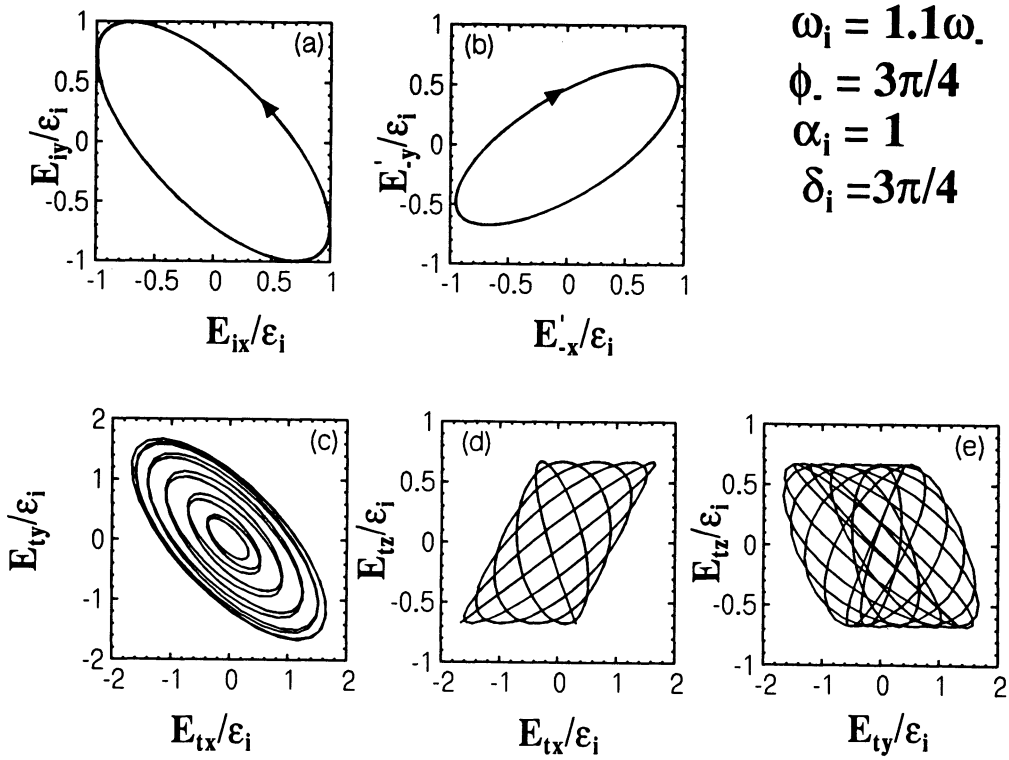

FIG. 6.—Parametric plot of electric fields E_i, E'_-, and E_t with respect to time t. Elliptically polarized incident wave E_i in the x-y plane (a); elliptically polarized scattered wave E'_- in the x'-y' plane (b); superimposed wave E_t in the x-y plane (c), x-z plane (d), and y-z plane (e).

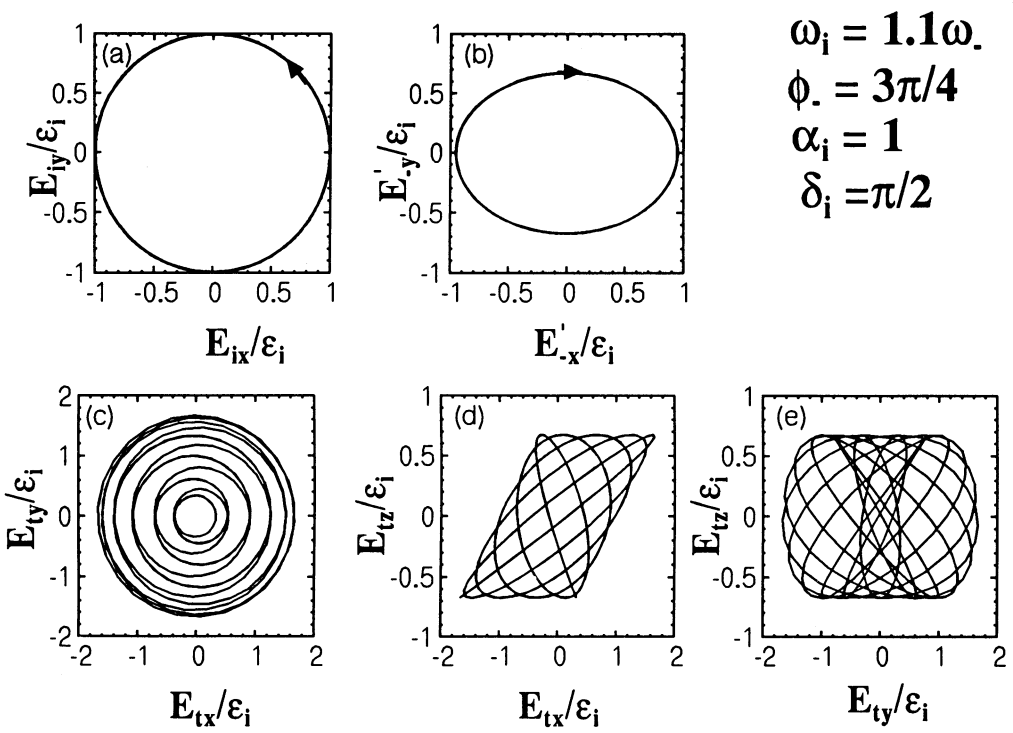

FIG. 7.—Parametric plot of electric fields E_i, E'_-, and E_t with respect to time t. Circularly polarized incident wave E_i in the x-y plane (*a*); elliptically polarized scattered wave E'_- in the x'-y' plane (*b*); superimposed wave E_t in the x-y plane (*c*), x-z plane (*d*), and y-z plane (*e*).

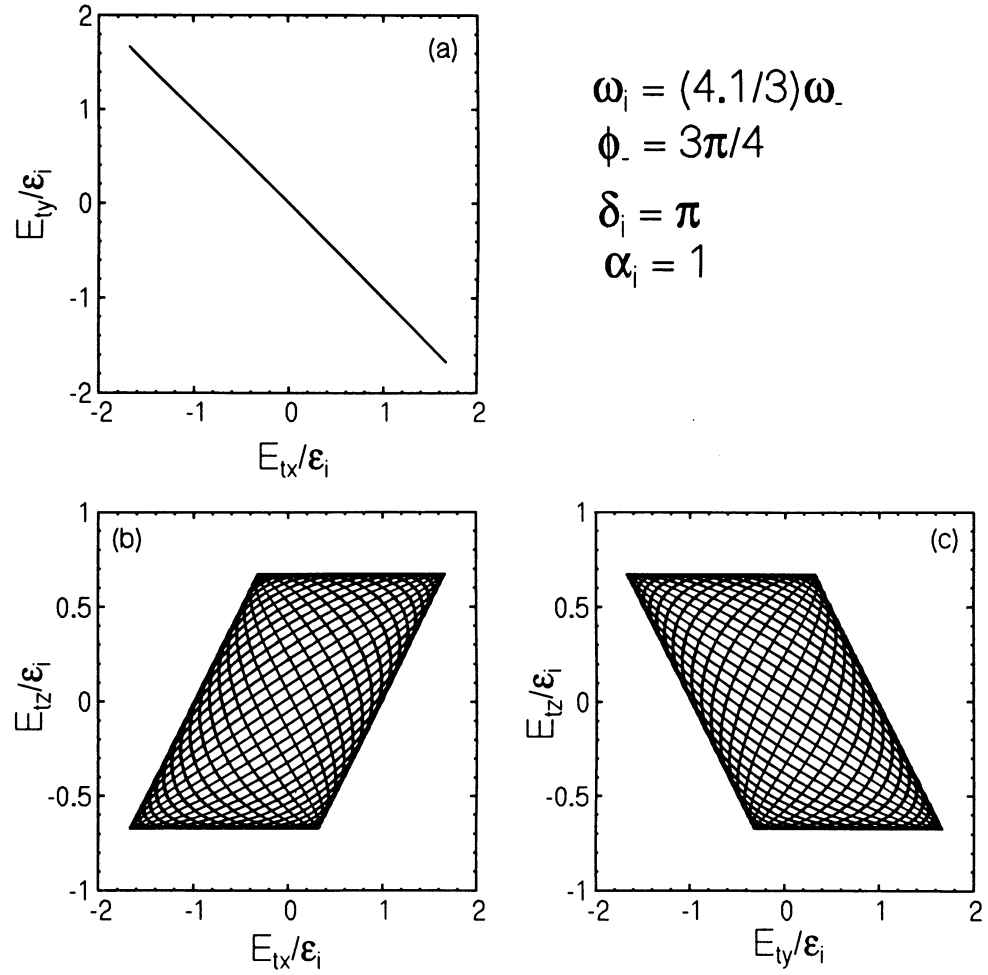

FIG. 8.—Parametric plot of electric field of the superimposed wave E_t with respect to time t, in the range $0 \le t \le 15T$. For $\omega_i/\omega_- = 4.1/3$, it shows a quasi-periodic pattern in the x-y plane (*a*), x-z plane (b), and y-z plane (*c*), when the incident wave is same as in Fig. 5*a*.

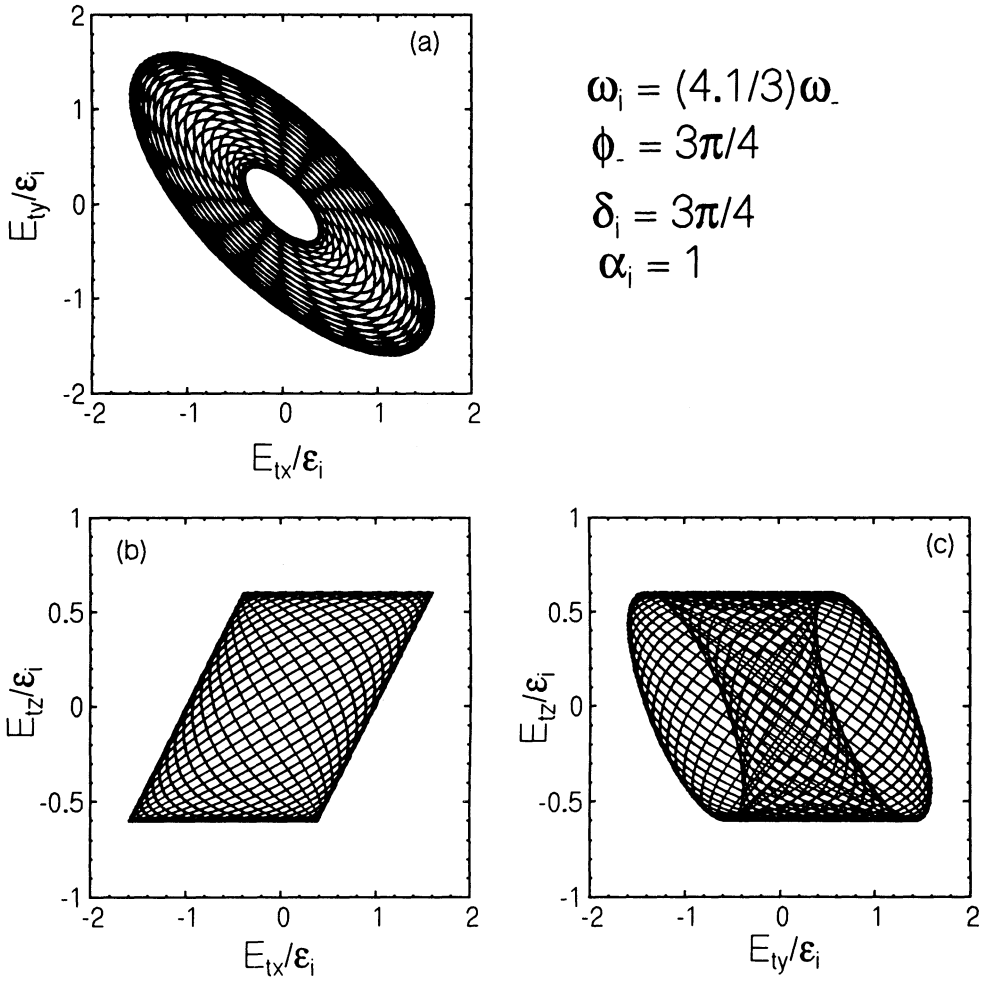

FIG. 9.—Parametric plot of electric field of the superimposed wave $\boldsymbol{E}_t$ with respect to time t, in the range $0 \leq t \leq 15T$. For $\omega_i/\omega_- = 4.1/3$, it shows a quasi-periodic pattern in the x-y plane (*a*), x-z plane (*b*), and y-z plane (*c*) when the incident wave is same as in Fig. 6*a*.

Figures 9*a*–9*c*, and Figures 7*c*–7*e* change to Figures 10*a*–10*c*, respectively. Figures 8, 9, and 10 show that E_t covers the entire x-y, x-z, and y-z planes with increasing time t. This ergodic behavior of $\boldsymbol{E}_t$, with increasing time t for an irrational ratio of ω_i to ω_-, is not yet chaotic (Milonni, Shih, & Ackerhalt 1987).

In the next case, if we consider the frequency ratio to be an integer, say $\omega_i/\omega_- = 2$, in Figure 7, then the components of $\boldsymbol{E}_t$ trace out Figures 11*c*–11*e*.

4.2. *In Quasars*

The typical values of the plasma and radiation parameters in the broad-line region, at a distance $r = r_{pc} \times 3 \times 10^{18}$ cm from the central engine of a quasar, are (Krishan & Wiita 1990; Gangadhara & Krishan 1992): electron density $n_e = n_{10} \times 10^{10}$ cm^{-3}, temperature $T_e = T_5 \times 10^5$ K, and luminosity $L = L_{42} \times 10^{42}$ ergs s in the radio band $\Delta\omega \approx \omega_{pe}$.

We know from the multifrequency observations of 3C 273 by Courvoisier et al. (1987) that $I_i = 4 \times 10^{-22}$ ergs cm^{-2} s^{-1} Hz^{-1} at the radio frequency $\nu_i = 6.4 \times 10^9$ Hz. For $\omega_i = 1.1\omega_-$, we obtain from equation (33) that $I_- = 1.8 \times 10^{-22}$ ergs cm^{-2} s^{-1} Hz^{-1}. Using these parameters, one can reproduce Figures 2–11 for quasar 3C 273.

4. FROM QUASI PERIODICITY TO CHAOS

The transition from two-frequency quasi periodicity to chaos has been observed in a variety of experiments, especially in fluid flows (Swinney & Gollub 1978). However, it is possible to have a one-frequency → two-frequency → three-frequency → chaos transition. Such a three-frequency route to chaos has been observed experimentally (Gollub & Benson 1980; Libchaber, Fauve, & Laroche 1983; Martin, Leber, & Martienssen 1984).

In 1978, Newhouse, Ruelle, & Takens argued that small perturbations (thermal) can cause the system to become unstable after the appearance of just three incommensurate frequencies. In other words, after the appearance of two incommensurate frequencies, a system is likely to become chaotic because small perturbations would destroy the three-frequency motion. This route to chaos is therefore referred sometimes as the two-frequency route (Milonni et al. 1987).

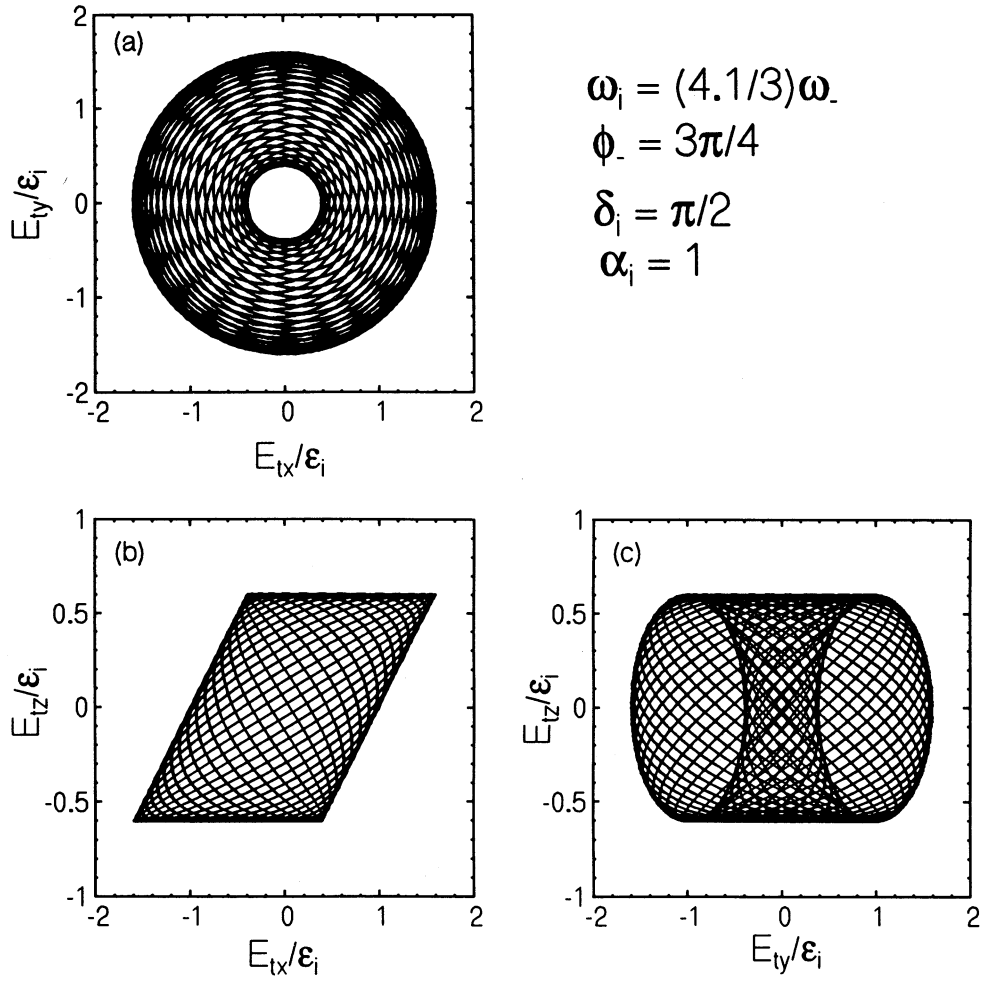

FIG. 10.—Parametric plot of electric field of the superimposed wave E_t with respect to time t, in the range $0 \le t \le 15T$. For $\omega_i/\omega_- = 4.1/3$, it shows a quasi-periodic pattern in the x-y plane (*a*), x-z plane (*b*), and y-z plane (*c*), when the incident wave is same as in Fig. 7*a*.

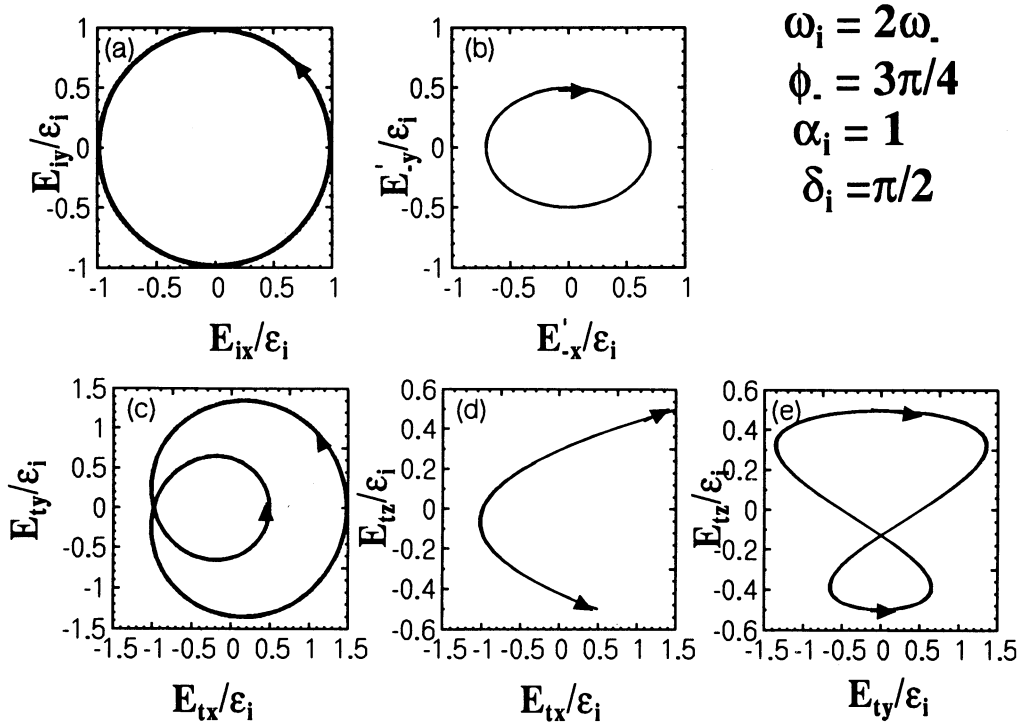

FIG. 11.—Parametric plot of electric fields E_i, E'_-, and E_t with respect to time t, using $\omega_i/\omega_- = 2$. Circularly polarized incident wave E_i in the x-y plane (*a*); elliptically polarized scattered wave E'_- in the x'-y' plane (*b*); superimposed wave E_t in the x-y plane (*c*), x-z plane (*d*), and y-z plane (*e*).

In forward Raman scattering, whenever the intensity of the incident electromagnetic wave is larger than a threshold which depends on damping mechanisms, the incident wave scatters into Stokes and anti-Stokes modes. These scattered electromagnetic waves can grow to intensities over the threshold value so that they also take part in further Raman process. Consequently, satellite modes with frequency shifts of some multiple of ω_{pe} can appear on both sides of a given high-frequency intensity incident line: this Raman cascade can lead to turbulence and plasma heating (Chen, Kaufman, & Watson 1972).

It is clear that we can get behavior that looks quite complicated by adding just a few sine waves of different frequencies, and so in the limit of an infinite number of frequencies we might call the system turbulent or chaotic. In other words, we would have a transition to chaos by frequency proliferation, which obtains by a cascading process and/or by the addition of thermal radiation to the Raman-scattered radiation, resulting in a chaotic variation of radiation characteristics like flux and polarization.

5. CONCLUSION

The frequency (ω_-) of the scattered radiation differs from that of the incident radiation by the electron plasma frequency (i.e., $\omega_- = \omega_i + \omega_{pe}$). The bunching of electrons occurs due to the electric field of Langmuir waves. These waves can order the electron motion by forcing them to form bunches over a length comparable to the Debye length. The characteristic signatures of bunching are manifest through the frequency change ($\omega_- - \omega_i$), which is equal to ω_{pe} in the case of SRS, is equal to zero in the case of Thomson scattering on electrons at rest, and is a function of the electron kinetic energy in the case of Compton scattering, as well as through a very large growth rate and the consequent rapid changes in polarization. The *e*-folding time of the Raman instability represents a characteristic time during which a significant change in the degree of polarization, sense, and rotation of plane of polarization takes place. Therefore, the observed variability time should be of the order of or a few times the *e*-folding time.

The superimposed EM wave $\boldsymbol{E}_t$ shows new types of polarization patterns for different values of the frequency ratio ω_i/ω_-, the incident-wave electric field components ratio $\alpha_i = E_{yi}/E_{xi}$ and its initial phase δ_i, and the scattering angle ϕ_-. Through SRS the clockwise-polarized radiation can change into counterclockwise-polarized radiation and vice versa. In addition, a circularly polarized wave can change into a linearly polarized, a circularly polarized, or an elliptically polarized wave or vice versa, depending on the value of ϕ_-.

If the ratio of the frequencies ω_i/ω_- is an irrational number, then $\boldsymbol{E}_t$ traces out a quasi-periodic structure of polarization. The Raman cascade of sideband modes or the modulation of a superimposed wave with thermal perturbations will lead to a turbulent spectrum with a large number of frequencies; as a result periodic → quasi-periodic → chaotic transitions in the rotation of the superimposed electromagnetic wave can take place.

It has been shown by Tamour (1973) and Thomson et al. (1974) that the effect of finite bandwidth $\Delta\omega_i$ of the incident field on the instability can be taken care of by replacing the damping rate of the sidebands Γ_L by $\Gamma_L + 2\xi \approx \Gamma_L + \Delta\omega_i$, where ξ is the number of phase jumps per unit time. This happens because Γ_L is a measure of the duration of time an electron is allowed to oscillate with the driving field before being knocked out of phase by a collision. The same effect results when the driving field suffers a phase shift, and the two effects are additive. Thus replacing Γ_L by $\Gamma_L + \Delta\omega_i$ certainly raises the threshold for the instability. If Γ is the growth rate due to a monochromatic pump at ω_i, then the actual growth rate Γ' due to the broad pump with a spectral width $\Delta\omega_i \gg \Gamma$ is given by $\Gamma' = \Gamma^2/\Delta\omega_i$ (Kruer 1988). Thus the reduction in the growth rate due to the finite bandwidth may be compensated to some extent by the large luminosity radiation believed to be generated by coherent emission processes. Hence, the presence of incoherence through finite bandwidth in the radiation field effectively increases the damping rates and the thresholds and, therefore, reduces the growth rate of SRS instability.

We have made some efforts to model the nonthermal continuum of quasars by combining the contributions from SRS and SCS processes. We have specifically proposed that the spectral break in the blue region may be due to the change in the process of emission from SRS to SCS (Krishan & Wiita 1990; Gangadhara & Krishan 1992). These proposals need to be investigated in more detail in a number of AGNs and quasars.

Features like a change in rotation of the polarization plane, sense reversal, and extremely rapid temporal changes would help to explain many observations for which existing mechanisms prove to be inadequate. Because of the very strong dependence of rotation angle on plasmas parameters via the growth rate, in an inhomogeneous plasma medium the depolarization is a natural outcome. A strong magnetic field can also affect the process: we intend to study this in detail in later work. We believe that a plasma process such as SRS along with the possible development of chaos may be a potential mechanism for polarization variability in high-energy sources.

V. K. would like to thank Professors A. N. Sessler and W. Leemans of the Lawrence Berkeley Laboratory for many very useful discussions.

REFERENCES

Aller, M. F., Aller, H. D., & Hughes, P. A. 1991, in Extragalactic Radio Sources—From Beams to Jets, 7th IAP Meeting, ed. J. Roland, H. Sol, & G. Pelletier (Cambridge: Cambridge Univ. Press), 167
Asséo, E., Pellat, R., & Sol. H. 1980, in IAU Symp. 95, Pulsars, ed. W. Sieber & R. Wielebinski (Dordrecht: Reidel), 111
Baker, D. N., Borovsky, J. E., Benford, G., & Eilek, J. A. 1988, ApJ, 326, 110
Beal, J. H. 1990, in Physical Processes in Hot Cosmic Plasmas, ed. W. Brinkmann (Dordrecht: Kluwer), 341
Benford, G. 1992, ApJ, 391, L59
Blandford, R. D., & Königl, A. 1979, ApJ, 232, 34
Burbidge, G. R., & Burbidge, E. M. 1967, Quasi-Stellar Objects (San Francisco: Freeman)
Chen, B. I., Kaufman, A. N., & Watson, K. M. 1972, Phys. Rev. Lett., 29, 581
Cordes, J. M. 1983, in Positron-Electron Pairs in Astrophysics, ed. M. L. Burns, A. K. Harding, & R. Ramaty (AIP Conf. Proc. 101), 98
Cotton, W. D., Gelzahler, B. J., Marcaide, J. M., Shapiro, I. I., & Sanroma, M. 1984, ApJ, 286, 503
Courvoisier, T. J.-L., et al. 1987, A&A, 176, 197
Drake, J. F., Kaw, P. K., Lee, Y. C., Schmidt, G., Liu, C. S., & Rosenbluth, M. N. 1974, Phys. Fluids, 17, 778

Fried, D., & Conte, S. D. 1961, The Plasma Dispersion Function (New York: Academic)
Gangadhara, R. T., & Krishan, V. 1992, MNRAS, 256, 111
———. 1993, ApJ, 415, 505
Gangadhara, R. T., Krishan, V., & Shukla, P. K. 1993, MNRAS, 262, 151
Gil, J. A., & Snakowsky, J. K. 1990a, A&A, 234, 237
———. 1990b, A&A, 234, 269
Gollub, J. P., & Benson, S. V. 1980, J. Fluid Mech., 100, 449
Hasegawa, A. 1978, Bell System Tech. J., 57, 3069
Krishan, V., & Gangadhara, R. T. 1992, in International Conference on Plasma Physics, Vol. 16c, Part 3, ed. W. Freysinger, K. Lackner, R. Schrittwieser, & L. Lindinger (Innsbruck: European Physical Soc.), 1671
Krishan, V., & Wiita, P. J. 1990, MNRAS, 246, 597
———. 1994, ApJ, 423, 172
Kruer, W. L. 1988, The Physics of Laser-Plasma Interactions (New York: Addison-Wesley)
Lesch, H., & Pohl, M. 1992, A&A, 254, 29
Libchaber, A., Fauve, S., & Laroche, C. 1983, Physica, 7D, 73
Liu, C. S., & Kaw, P. K. 1976, Adv. Plasma Phys., 6, 83
Manchester, R. N., & Taylor, J. H. 1977, Pulsars (San Francisco: Freeman)
Martin, S., Leber, H., & Martienssen, W. 1984, Phys. Rev. Lett., 53, 303
Melrose, D. B. 1978, ApJ, 225, 557
Milonni, P. W., Shih, M.-L., & Ackerhalt, J. R. 1987, Chaos in Laser-Matter Interactions (Singapore: World Scientific)
Newhouse, S. E., Ruelle, D., & Takens, F. 1978, Commun. Math. Phys., 64, 35
Ruderman, M., & Sutherland, P. 1975, ApJ, 196, 51
Sillanpää, A., Nilsson, K., & Takalo, L. O. 1991, in Extragalactic Radio Sources—From Beams to Jets, 7th IAP Meeting, ed. J. Roland, H. Sol, & G. Pelletier (Cambridge: Cambridge Univ. Press), 174
Stockman, H. S. 1978, in Pittsburgh Conf. on BL Lac Objects, ed. A. M. Wolfe (Pittsburgh: Univ. Pittsburgh Press), 149
Swinney, H. L., & Gollub, J. P. 1978, Phys. Today, 31, 41
Tamour, S. 1973, Phys. Fluids, 16, 1169
Thomson, J. J., Kruer, W. L., Bodner, S. E., & DeGroot, J. 1974, Phys. Fluids, 17, 849
van der Laan, H. 1966, Nature, 211, 1131
Weatherall, J. C., & Benford, G. 1991, ApJ, 378, 543
Weiland, J., & Wilhelmsson, H. 1977, Coherent Non-Linear Interaction of Waves in Plasmas (New York: Pergamon), 60